Available online at www.sciencedirect.com

ScienceDirect

Proceedings of the Combustion Institute 35 (2015) 1709–1716

Proceedings of the Combustion Institute

www.elsevier.com/locate/proci

The effect of support fibers on micro-convection in droplet combustion experiments

Y.C. Liu [a,*], Y. Xu [a], C.T. Avedisian [a], M.C. Hicks [b]

[a] Sibley School of Mechanical and Aerospace Engineering, Cornell University, Ithaca, NY 14853, USA
[b] NASA Glenn Research Center, Mail Stop 77-5, 21000 Brookpark Road, Cleveland, OH 44135, USA

Available online 4 August 2014

Abstract

This study reports experimental evidence of gas phase micro-convection induced by support fibers used in droplet combustion experimentation. Soot aggregates formed during combustion of n-octane and n-decane droplets (initial diameters ranging from 0.5 mm to 5 mm) provide natural seeds to reveal the thermal and flow asymmetries involved. The experiments are carried out in an environment that reduces the influence of forced and buoyant convection for both free-floating (unsupported) and fiber-supported droplets. Under these conditions, the soot trapping patterns (due to a balance of thermophoretic and flow-induced drag) would be spherical. However, this situation is only observed for unsupported droplets, or for fiber-supported droplets when the fiber is small relative to the droplet diameter. For $D_o < 1$ mm a ground based drop tower employed two 14 μm diameter SiC fibers to fix the droplet's position during burning; unsupported droplets were also examined. For $D_o > 1$ mm the International Space Station provided capabilities for anchoring test droplets onto a single 80 μm SiC fiber, and for deploying unsupported droplets. Results clearly indicate that a non-symmetric gas flow field exists in some cases (i.e., for 1 mm $< D_o <$ 3 mm, with an 80 μm fiber) near to where the fiber enters the droplet. This gas motion originates from the presence of the fiber that introduces asymmetries in the temperature and flow fields resulting in localized force imbalances on the soot particles, which cause vortical flow patterns near the fiber. This may in part be explained by flow asymmetries induced by droplet shape distortions coupled with heat exchanges between the fiber and surrounding gas and conduction into the droplet, resulting in a Marangoni flow near the droplet surface. For very small fibers (or for unsupported droplets) spherical soot shells are found suggesting that no thermal and flow asymmetries exist.

Keywords: droplet combustion; experiment; low gravity; fiber effect; heat transfer

1. Introduction

The understanding of liquid fuel combustion has historically relied on experiments carried out on both droplet and spray flames [1,2] and their performance in engines. It has long been recognized that isolated droplets burning in an environment that promotes spherical symmetry retains

* Corresponding author. Address: Department of Computer Science, Engineering and Physics, University of Michigan-Flint, Flint Township, MI 48502, USA.
E-mail address: yl677@cornell.edu (Y.C. Liu).

http://dx.doi.org/10.1016/j.proci.2014.07.022
1540-7489/

many physical processes found in spray flames [3]. The spherical symmetry that results when external convective effects are reduced is the base case of liquid fuel combustion [4] and is most attractive for modeling [5–7].

At one end are experiments from which the complete burning history of free-floating fuel droplets can be observed. The challenge here is to restrict drift of the droplet during the burning process that may result in it moving out of the imaging field of view [8,9]. This problem can be significant if not one of the most difficult to overcome in droplet combustion experimentation. The other configuration is a droplet physically anchored to some sort of support structure to restrict its motion, which is the most often utilized configuration in droplet combustion experimentation [4,6–11]. The efficacy of the data obtained rests on the support structure exerting a minimal effect [12,13] on burning such that the combustion properties that result (e.g., burning rate, flame diameter, etc.) will be nearly the same as for a droplet burning without benefit of a support structure to restrict its motion.

The most common explanation for a support structure's influence on droplet burning is heat conduction through the fiber [14–20]. The fiber can also create gas phase temperature asymmetries around the droplet which can extend to the droplet surface and induce Marangoni internal flow in the liquid [21]. Another potential influence is the droplet shape. The shape of a droplet supported by a fiber can be non-spherical which itself can create flow asymmetries because the Stefan flow originates at the droplet surface and is normal to it there [9]. Without a fiber, the flow streamlines would resemble the spokes of a wheel.

This paper reports a study of the thermal and transport asymmetries developed in fiber-supported stationary droplet combustion experiments carried out in a low gravity environment to remove the influence of buoyancy. Results are compared to free or unsupported droplets where the transport process is more symmetric. The droplets are mounted onto the middle of a SiC fiber which is considered to reduce flow and thermal asymmetries compared to a droplet hanging at the tip of a single fiber [9]. The initial droplet diameter (D_o) is varied over the range 0.5 mm to 5 mm in the standard atmospheric with fiber support diameters fixed at either 14 μm for $D_o < 1$ mm or 80 μm for $D_o > 1.8$ mm resulting in $22 < D_o/D_{fiber} < 65$. For these smaller values of D_o/D_{fiber} significant asymmetric flows are observed in the gas phase.

The experiments for $D_o < 1$ mm were carried out in a ground-based (GB) drop tower while for 1.8 mm $< D_o <$ 5 mm an experimental facility aboard the International Space Station (ISS) was used. Both unsupported and fiber-supported experiments were performed. The fuels selected for study are n-octane and n-decane, in part because they are mildly sooting thus allowing quantitative measurements of droplet, flame and soot shell diameter (i.e., extensive sooting would obscure the droplet visibility and be problematic for data analysis of more heavily sooting fuels). The soot particles are used as a natural seeding of the flow to reveal non-symmetric thermal fields.

2. Experimental methods

2.1. Ground-based experiments

A 7.6 m drop tower is used to create a low gravity condition (for 1.2 s) that promotes spherical symmetry for the droplet flame. Figure 1a shows the layout of the instrumentation package for drop tower experiments and Fig. 1b shows experimental procedures for a drop tower experiment. For fiber-supported experiments, a test droplet (n-decane) is deployed onto the intersection of two SiC (14 μm) fibers before the package is released into free fall. The droplet is ignited by two parallel symmetric sparks at the opposite sides. The spark ignition energy is about 0.1 J. For n-decane, the chemical energy is about 44×10^6 J/kg. The mass of a nominally 0.5 mm droplet is $\sim 4.6\times10^{-8}$ kg. The combustion heat

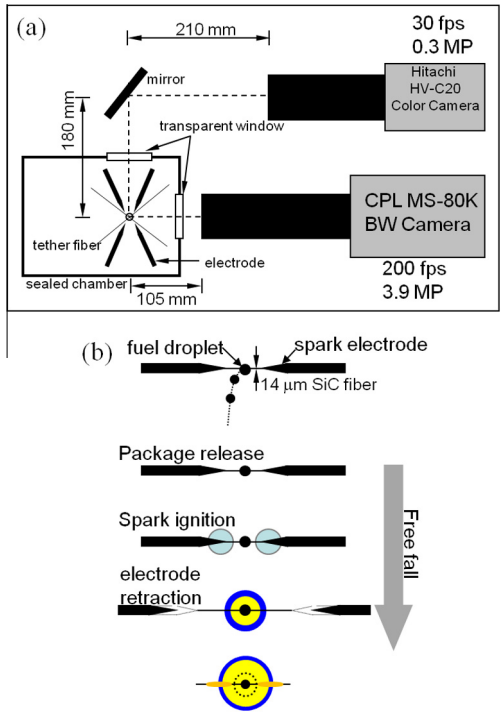

Fig. 1. (a) Schematic of the instrumentation package for drop tower experiment; (b) experimental sequence.

release therefore is then about 2.0 J, or 20 times larger than the spark ignition energy. A 320 ms delay time is deliberately made for the sparks to avoid the initial shaking of the package that may transmit to the droplet through the fibers.

For free droplet experiments (i.e. no supporting fibers), a modification of a procedure previously developed [22] is used. The test droplet is propelled in a vertical trajectory and the package is released when the droplet reaches its apex. With proper timing, the droplet flame can have minimal motion during a burn. The precision in positioning and the timing of the release of the package is critical for success.

Digital video images showing both the droplet and soot configuration were obtained by a black-and-white (BW) camera (200 fps, 3.9 megapixels (MP)), backlit by a 1 W LED. Flame images (self-illuminated) showing the flame structure and shape were obtained with a color camera (30 fps, 0.3 MP) [23]. Detailed methods for image analyses and measurements are described elsewhere [23,24]. The uncertainty of the measured GB droplet diameters are ± 1.8% initially and ± 11% at the end of burning; for the soot shell, ± 4.3% initially and ± 13% at the end; and for the GB flame diameters, ± 3.7% initially and ± 6.4% at the end.

2.2. Space-based experiments

Experiments on the ISS were carried out using the Multi-user Droplet Combustion Apparatus (MDCA) that is installed in the Combustion Integrated Rack (CIR). Detailed hardware descriptions can be found elsewhere [25–28]. Figure 2 is a schematic of the experimental hardware for the ISS droplet combustion experiments. A deployment motor transmits liquid fuels from a fuel tank to the tips of two needles where the droplet is "bridged" due to surface tension. A single fiber (SiC, 80 μm) can be optionally placed between the two needle tips to tether the test droplet (n-octane and n-decane). An experiment is initiated by retracting the two deployment needles followed by droplet ignition using two hot-wire igniters. An ideal needle retraction event allows the droplet to stay in the same position with no directional motion.

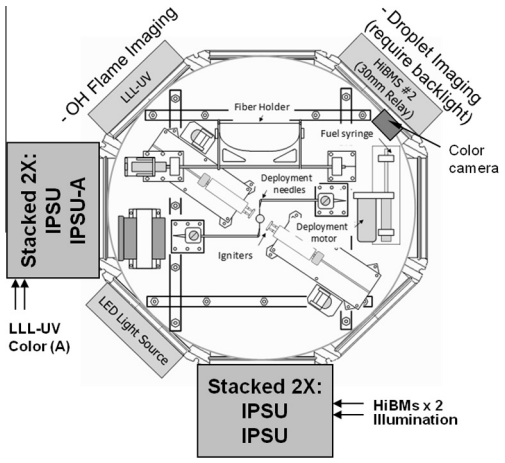

Fig. 2. Schematic of the Multi-user Droplet Combustion Apparatus of the ISS.

The entire droplet burning process is recorded by a High Bit-Depth Multispectral (HiBMs) Package (1 MP) (backlit by a light source with a center wavelength between 650 - 660 nm) and a color camera (0.3 MP) with both cameras having a frame rate of 30 fps. Only the droplet diameter data extracted from BW images [22,23] are reported in this study. The uncertainty of droplet size measurements for the ISS experiments are ± 1.8% initially and ± 7.5% at the end of a burn.

3. Results and discussions

3.1. Droplet flame structure

Figure 3 compares fiber-supported (14 μm fibers) and free droplet flames for 0.5 mm n-decane droplets. With the absence of the support fiber, the soot shell around the free droplet is denser compared to the fiber-supported droplet. Soot agglomerates are found on the soot shell at 0.2 s for free droplet (cf. Fig. 3d). In contrast, Fig. 3c shows that soot aggregates tend to attach to the support fiber such that the soot shell appears less intense during a burn.

Figure 4 shows the evolution of D^2 for one run of a fiber-supported droplet and data from three repetitions of free droplet experiments. The fiber-supported and freely deployed droplet data are almost identical suggesting that the effects of a fiber on the droplet combustion rate are minimal for $D_o \approx 0.5$ mm. The free droplet data are slightly more scattered in the early burning period indicating small droplet distortion due to the impact of the sparks on the free floating droplets. This effect is significantly diminished for fiber supported droplets.

A spark discharge can influence the thermal field surrounding a droplet. For estimation purposes a region of influence of the spark, δ, is estimated by assuming that an electrode is like a semi-infinite solid. The hot gas region is the estimated as $\delta \sim (\alpha_g\, t)^{1/2}$. Using a thermal diffusivity of air at 1000 K ($\alpha_g \sim 10^{-4}$ m^2/s) and a spark "on" time of 0.8 ms, δ ~0.3 mm which is an order of magnitude smaller than the average flame diameter.

Figure 5 shows the flame standoff ratio (FSR = D_f/D) and soot standoff ratio (SSR = D_s/D) obtained from ground-based fiber-supported and free droplet experiments. The FSR monotonically

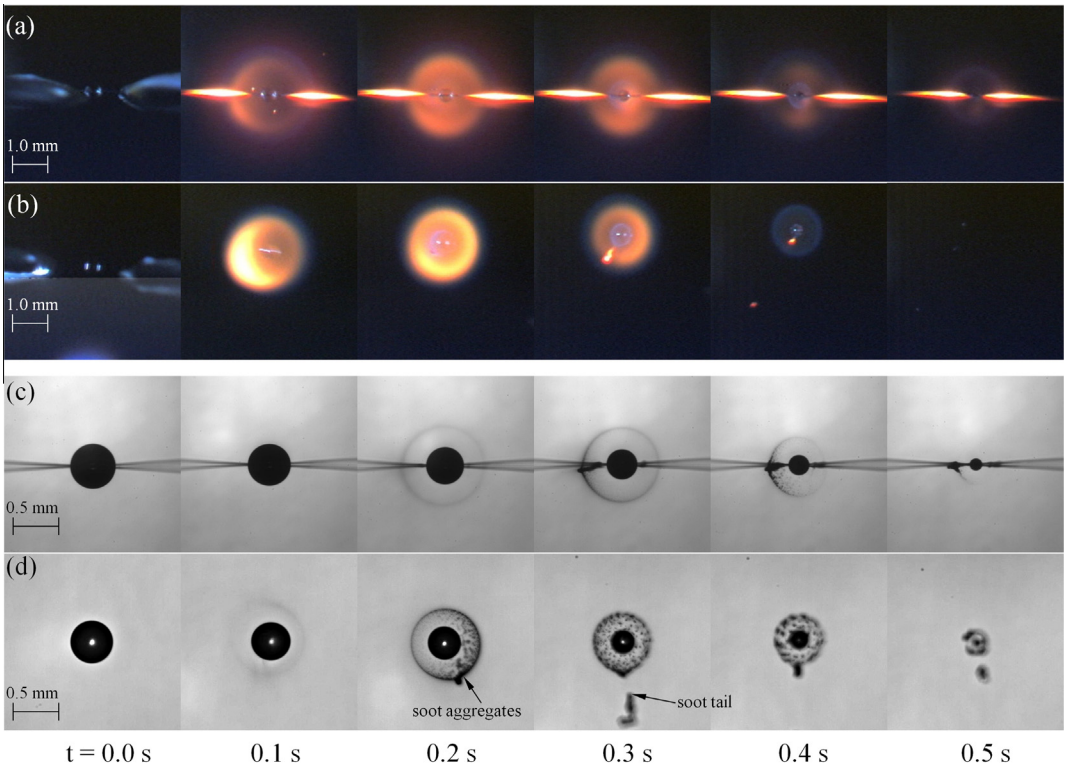

Fig. 3. Photographs of n-decane droplets burning (a) with support fibers (color); (b) without support fibers (color); (c) with support fibers (BW); (d) without support fibers (color). D_o for (a) and (c) is 0.54 mm, for (b) and (d) it is 0.51 mm. (For interpretation of the references to colour in this figure legend, the reader is referred to the web version of this article.)

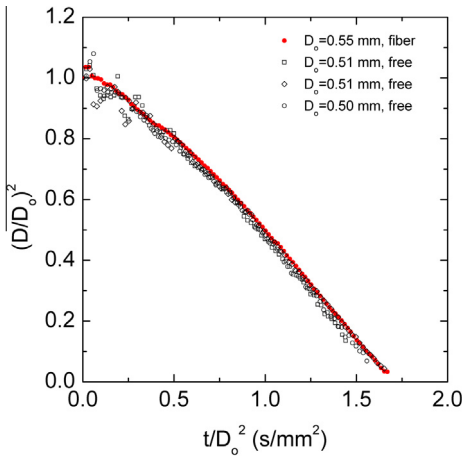

Fig. 4. Evolution of D^2 for a fiber-supported n-decane droplet and three free-droplets (D_{fiber} = 14 μm).

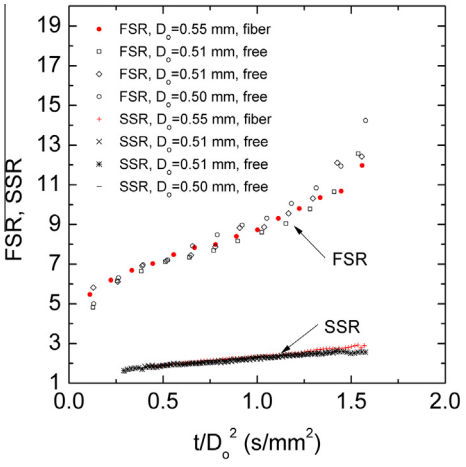

Fig. 5. Evolution of D_f/D and D_s/D of a n-decane fiber-supported (D_{fiber} = 14 μm) droplet and three free-droplets.

increases during the burning process. Except near the end, the fiber-supported data (red close symbols) overlap with the free droplet data (white open symbols) for the entire burning. Comparing the FSR suggests no difference between the two experimental setups. Regarding the SSR, though all the data appear, the fiber-supported SSR measurements are slightly higher than the free droplet data when $t/D_o^2 > 1$ s/mm^2. This difference may be due to soot aggregates easily escaping the flame for free droplets while they remain on the fiber

with their motion restricted for fiber-supported droplets.

For the ISS "large" droplet experiments (1.8 mm < D_o < 5 mm) free and fiber-supported droplet flame configurations are compared in Figs. 6 and 7. For a 2.64 mm initial diameter fiber-supported n-octane droplet in the ISS (Fig. 6a), the soot shell is significantly distorted and stretched in a direction perpendicular to the fiber, yet the spherical symmetry of the flame remains largely unaffected. The soot particle trajectories suggest a "vortex-like" flow structure near the droplet-fiber intersection. Figures 8b and 8c show enlarged views of fiber-supported n-octane and n-decane droplets, respectively, that further illustrate the significant asymmetries of the soot trajectories by the fiber. A micro-convection flow pattern is suggested by the soot aggregates following a vortex-like gas transport configuration. The unsupported n-octane droplets shown in Figs. 6b and 6c from the ISS experiments, along with an n-decane droplet from the ground-based experiments (Fig. 8a, D_o = 0.51 mm) show no significant asymmetries in the soot trapping patterns. Similar trends are followed by the n-decane droplets in Figs. 7c and 7d: free droplets show reasonably symmetrical soot configurations and, by inference, gas flow patterns while fiber-supported droplets do not for the fiber diameter used in the ISS experiments at the D_o values.

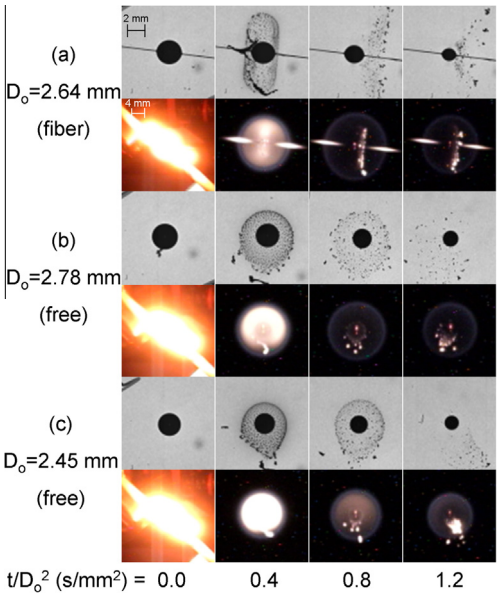

Fig. 6. BW and color photographs of n-octane droplet burning on the ISS: (a) D_o = 2.64 mm (D_{fiber} = 80 μm); (b) D_o = 2.78 mm (unsupported); (c) D_o = 2.45 mm (unsupported). (For interpretation of the references to colour in this figure legend, the reader is referred to the web version of this article.)

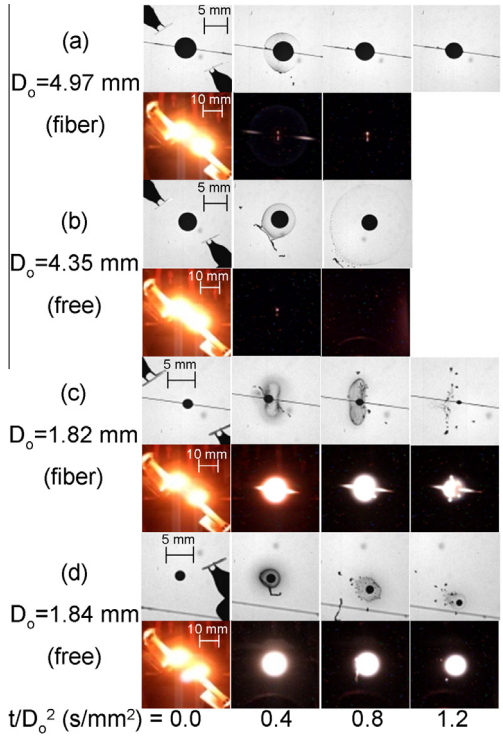

Fig. 7. BW and color photographs of n-decane droplet burning on the ISS: (a) D_o = 4.97 mm (D_{fiber} = 80 μm); (b) D_o = 4.35 mm (unsupported); (c) D_o = 1.82 mm (D_{fiber} = 80 μm); (d) D_o = 1.84 mm (unsupported). (For interpretation of the references to colour in this figure legend, the reader is referred to the web version of this article.)

For the larger n-decane droplets the presence of the fiber essentially had no substantive effect on the soot shell (D_o = 4∼5 mm in Figs. 7a,b). Fiber-induced flow patterns, as traced by soot aggregates near the fiber, are seen for small n-decane droplets (D_o = 1.82 mm, Fig. 7c), while Fig. 7d shows that for free droplets the spherical symmetry of the soot shell and flame is reasonably well maintained. For larger free droplets the spherical symmetry of the soot shell and flame is reasonably well maintained. For larger free droplets in the ISS apparatus the effects of droplet drift after deployment on the flow symmetry (as revealed by the soot aggregates acting as seeds of the flow) are minimal as the droplets are evidently moving too slowly. Soot asymmetries noted in some ISS images can be induced by the physical retraction of the igniters though such influences are much smaller for the GB spark-ignited droplets (cf, Fig. 3).

3.2. Quantitative data

Figures 9 and 10 show the evolutions of D^2, normalized by D_o^2, as obtained from fiber-supported and free droplet data (Figs. 6 and 7) for

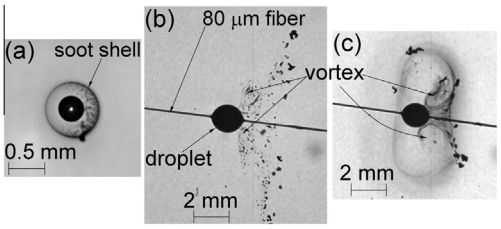

Fig. 8. Photographs of instantaneous soot aggregates that reveal soot aggregate patterns (a) n-decane (unsupported with spherical symmetry), $D_o = 0.51$ mm, $t = 0.2$ s; (b) n-octane, $D_o = 2.64$ mm, $D_{fiber} = 80$ μm, $t/D_o^2 = 1.0$ s/mm^2; (c) n-decane, $D_o = 1.82$ mm, $D_{fiber} = 80$ μm, $t/D_o^2 = 0.4$ s/mm^2.

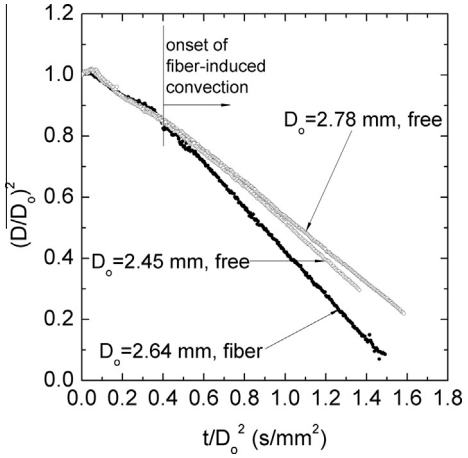

Fig. 9. Evolution of D^2 for n-octane droplets burning with and without 80 μm SiC support fibers.

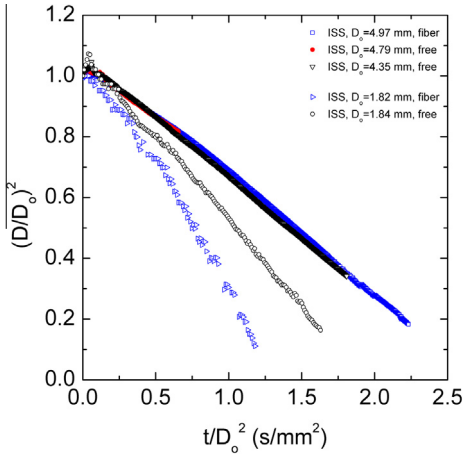

Fig. 10. Evolution of D^2 for n-decane droplets burning with and without 80 μm SiC support fibers.

n-octane and n-decane, respectively. Considerably higher burning rates ($K = -d((D/D_o)^2)/d(t/D_o^2)$) are found for fiber-supported experiments (cf. Fig. 9, $D_o = 2.64$ mm; Fig. 10 $D_o = 1.82$ mm) compared to free droplets with similar D_o. The fiber effects emerge later in the burning process for a slightly larger droplet ($D_o = 2.64$ mm, at $t/D_o^2 \sim 0.4$ s/mm^2 (Fig. 9)), compared to a smaller droplet ($D_o = 1.82$ mm, at $t/D_o^2 \sim 0.2$ s/mm^2 (Fig. 10)). Before the droplet drifted out of the camera view or extinguished, the data for free droplets for the largest diameters ($D_o = 4.97$ mm) are very close to the fiber data ($D_o = 4.35$ mm) due to the fact that the size of the fiber is relatively small compared to the droplet. Figure 9 shows that the evolution of D^2 for fiber-supported and free droplets are close for $t/D_o^2 < 0.4$ s/mm^2, which is consistent with Fig. 4 where $D_o/D_{fiber} \sim 36$ while for Fig. 9 $D_o/D_{fiber} \sim 33$. Deviations between free and fiber configurations appear to coincide with the onset of convection (cf, Fig. 6a).

The influence of the support fiber on droplet burning is better understood from the visualizations provided by the photographic images of the sooting patterns that result. Figure 8 shows enlarged images from representative free droplet (a) and fiber-supported experiments (b and c). As seen in Fig. 8a, the soot aggregates form a spherical shell defined by the location where the radially outward Stephan-flow drag forces are equal to the radially inward thermophoretic forces. In this case the flow field is thermally symmetric. With a fiber (Figs. 8b and 8c) it is evident that spherical soot shells no longer are formed. At the same time, the droplet is clearly not spherical.

The influence of droplet shape on non-symmetric flow patterns deserves to be mentioned as well. Streamlines of the evaporation-induced vapor flow at the droplet are orthogonal to the droplet surface. To the extent that the droplet shape is not spherical the streamlines of the flow induced by evaporation will not be symmetric either. The soot trapping patterns will also not be symmetric (i.e., for a spherical shell).

In addition, the non-uniform temperature at the droplet surface that results from additional heating by the fiber at the droplet-fiber interface may induce surface tension gradients and therefore Marangoni flows. This Marangoni effect may lead to fluid motion inside the droplet and thus a component of the gas velocity at the droplet surface that is no longer normal to the droplet surface. The corresponding force on soot aggregates trapped to produce the unusual, vortex-like, patterns observed. The soot aggregates are effective at essentially seeding the flow allowing visualization of this non-symmetric gas flow pattern and vortex-like motion observed near the fiber.

An alternative explanation for the vortex-like structure might be that the presence of the fiber itself introduces thermal asymmetries in the gas phase resulting in an increase in the thermophoretic forces acting on the soot particles, driving them radially inward despite the radially outward

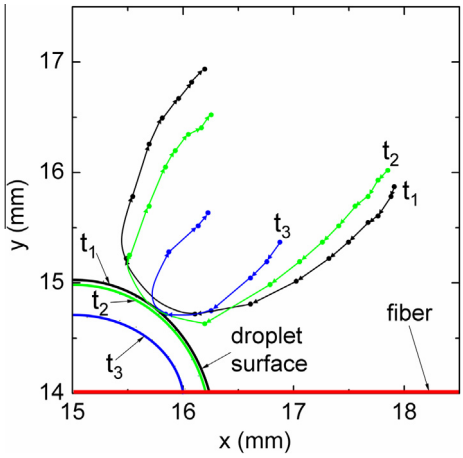

Fig. 11. Trajectories of three soot aggregates for an n-octane droplet beginning at the indicated times after ignition: $t_1 = 4.47$ s, $t_2 = 5.43$ s, $t_3 = 8.27$ s ($D_o = 2.64$, $D_{fiber} = 80$ μm).

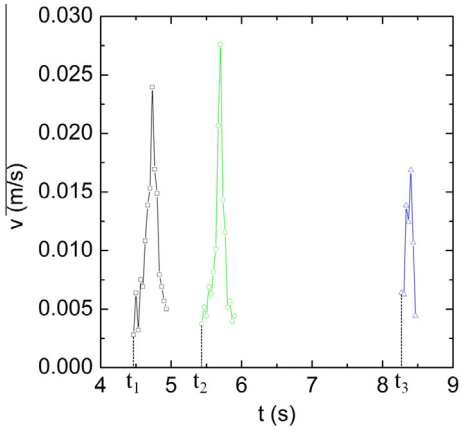

Fig. 12. Velocities of three soot aggregates for an n-octane droplet beginning at the indicated times after ignition: $t_1 = 4.47$ s, $t_2 = 5.43$ s, $t_3 = 8.27$ s ($D_o = 2.64$, $D_{fiber} = 80$ μm).

flow-induced drag forces. In this case, the moving soot aggregates may actually drag the ambient gases along their thermophoretically driven trajectories, possibly enhancing the magnitude of the observed vortical flow.

Some quantitative measurements of the soot aggregate trajectories and velocities were made and are shown in Fig. 11. The trajectories of three separate aggregates were tracked for an n-octane droplet with $D_o = 2.64$ mm from an ISS experiment (Fig. 9). The indicated times (t_1 to t_3) are the times after ignition. The length of the arrows is a measure of the aggregate velocity. The inward motion of aggregates and the reversal of the trajectories as they approach the droplet surface is evident. Figure 12 shows the aggregate velocities. Interestingly, the aggregate velocity is highest (Fig. 12) where the trajectory is reversed (Fig. 11, arrows of longest length). As aggregates approach the droplet they begin to feel the effects of the Stefan velocity (v_g) which is estimated from Fig. 9 based on a burning rate (K) in the linear portion of the data. Taking $K \sim 0.7$ mm^2/s from Fig. 8 and estimating v_g from the classical droplet burning theory as $v_g \sim \frac{\rho_L}{\rho_g}\frac{K}{4D}$ we find (using properties of octane and air) that $v_g \sim 0.09$ m/s. A velocity of this magnitude would be sufficient to alter the aggregate trajectory, as the aggregate approaches the droplet surface.

4. Conclusions

Fiber-supported and free droplet experimental results indicated that for $D_o \sim 0.5$ mm n-decane droplets supported by 14 μm SiC fibers, no substantive influence of any asymmetric convection was revealed by soot trapping, which was in a nearly spherical pattern around the droplet. In these cases the thermal and flow fields were considered to be nearly spherically symmetric and no significant differences were found in the evolutions of D^2, FSR, and SSR between fiber-supported and unsupported droplets, except very near the end of burning where the droplet diameter approached the fiber diameter.

For droplets in the range of 1 to 3 mm supported by an 80 μm fiber, gas flows were altered near where the fiber enters the droplet as evidenced by vortical motion of the soot aggregates. Alterations in the gas flow (over and above that due to evaporation) may also be augmented by the presence of an asymmetric temperature field induced by the fiber through convective heating between the fiber and surrounding gas as well as conductive heating into the droplet that can promote a Marangoni flow field inside the droplet and which, by viscous drag, imparts a momentum into the gas at the droplet/vapor interface. Above $D_o = 3$ mm, soot shells were nearly spherical indicating a minimal influence of the fiber, and with no substantive differences between free and fiber supported droplets. The exact mechanism explaining the observed flow disturbances, determination of a threshold droplet/fiber diameter, and the subsequent effect on droplet burning rates continues to be a matter of speculation and requires further analysis.

Acknowledgments

This project is supported by NASA under the Grant No. NNX08AI51G. We thank all the NASA/FLEX team members including D.L. Dietrich (NASA Glenn), V. Nayagam (NASA Glenn), F.A. Williams (UCSD), F.L. Dryer (Princeton), B.D. Shaw (UC Davis), M. Y. Choi

(U Conn), T. Farouk (U South Carolina), P. Ferkul (NASA Glenn), for the discussion and assistance for the ISS experiments and image analyses. The assistance of Koffi Trenou and Jeff Rah of Cornell University with the ground-based experiments and image analyses is also appreciated.

References

[1] G.A.E. Godsave, Symp. (Int.) Combust. 4 (1953) 818–830.
[2] D.B. Spalding, Symp. (Int.) Combust. 4 (1953) 847–864.
[3] W.A. Sirignano, *Prog. Energy Combust. Sci.* 9 (1983) 291–322.
[4] Y.C. Liu, C.T. Avedisian, *Combust. Flame* 159 (2012) 770–783.
[5] A. Cuoci, M. Mehl, G. Buzzi-Ferraris, T. Faravelli, D. Manca, E. Ranzi, *Combust. Flame* 143 (2005) 211–226.
[6] Y.C. Liu, T. Farouk, A.J. Savas, F.L. Dryer, C.T. Avedisian, *Combust. Flame* 160 (2013) 641–655.
[7] T.I. Farouk, Y.C. Liu, A.J. Savas, C.T. Avedisian, F.L. Dryer, *Proc. Combust. Inst.* 34 (2013) 1609–1616.
[8] S. Kumagai, T. Sakai, S. Okajima, Symp. (Int.) Combust. 13 (1971) 779–785.
[9] C.T. Avedisian, G.S. Jackson, *J. Propul. Power* 16 (2000) 974–979.
[10] S. Nakaya, K. Fujishima, M. Tsue, M. Kono, D. Segawa, *Proc. Combust. Inst.* 34 (2013) 1601–1608.
[11] H. Nomura, H. Takahashi, Y. Suganuma, M. Kikuchi, *Proc. Combust. Inst.* 34 (2013) 1593–1600.
[12] J.H. Bae, C.T. Avedisian, *Combust. Flame* 137 (2004) 148–162.
[13] G.S. Jackson, C.T. Avedisian, *Proc. R. Soc. Lond. A* 446 (1994) 255–276.
[14] J.R. Yang, S.C. Wong, *Int. J. Heat Mass Trans* 45 (2002) 4589–4598.
[15] M. Mikami, H. Oyagi, N. Kojima, M. Kikuchi, Y. Wakashima, S. Yoda, *Combust. Flame* 141 (2005) 241–252.
[16] C. Chauveau, F. Halter, A. Lalonde, I. Gökalp, ILASS, Como Lake, Italy, Sep. 8–10, 2008, paper ID ILASS08-4-1.
[17] M.C. Hicks, V. Nayagam, F.A. Williams, *Combust. Flame* 157 (2010) 1439–1445.
[18] T. Farouk, F.L. Dryer, *Combust. Flame* 159 (2012) 200–209.
[19] A.T. Shih, C.M. Megaridis, *Combust. Flame* 102 (1995) 256–270.
[20] M. Mikami, M. Kono, J. Sato, D.L. Dietrich, F.A. Williams, *Combust. Sci. Technol.* 90 (1993) 111–123.
[21] N. Ghata, B.D. Shaw, 8th US National Combustion Meeting, Utah, May 19–22, 2013, Paper # 070HE-0020.
[22] C.T. Avedisian, B.J. Callahan, *Proc. Combust. Inst.* 28 (2000) 991–997.
[23] Y.C. Liu, Ph.D. Thesis, "Droplet combustion of surrogate and real fuel systems in a low convection condition: ground-based and space-based experiments," Sibley School of Mechanical and Aerospace Engineering, Cornell University, Ithaca, NY 14850, Aug. 2013.
[24] C.L. Dembia, Y.C. Liu, C.T. Avedisian, *Image Anal. Stereol.* 31 (2012) 137–148.
[25] B. Banu, Fluids and combustion facility (FCF) and combustion integrated rack (CIR). Payload Accomodations Handbook CIR-DOC-4064, NASA John H. Glenn Research Center, Cleveland, Ohio, 2008.
[26] J. Robbins J, C. Shinn, Multi-user droplet combustion apparatus flex2. Reflight Safety Data Package MDC-DOC-1790A, NASA John H. Glenn Research Center, Cleveland, Ohio, 2010.
[27] F.A. Williams, M.C. Hicks, V. Nayagam, M.Y. Choi, F.L. Dryer, B.D. Shaw, Research Requirements Document- Droplet Flame Extinguishment in Microgravity (FLEX), No. 4, NASA John H. Glenn Research Center, Cleveland, Ohio, 2005.
[28] D. L. Dietrich, V. Nayagam, M. C. Hicks, P. V. Ferkul, F. L. Dryer, T. Farouk, B. D. Shaw, H. K. Suh, M. Y. Choi, Y. C. Liu, C. T. Avedisian, F. A. Williams, NASA/TP-2013-216046, NASA John H. Glenn Research Center, Cleveland, Ohio (also, Microgravity Science and Technology, in press, 2014.).